

THE FORMATION AND PHYSICAL ORIGIN OF HIGHLY IONIZED COOLING GAS

RONGMON BORDOLOI^{1,2}, TIMOTHY M. HECKMAN³, & COLIN A. NORMAN^{3,4}*Draft version July 29, 2016*

ABSTRACT

We present a physically clear cooling flow theory that explains the origin of warm diffuse gas seen primarily as highly ionized absorption line systems in the spectra of background sources. We predict the observed column densities of several highly ionized transitions such as O VI, O VII, Ne VIII, N V, and Mg X; and present a unified comparison of the model predictions with absorption lines seen in the Milky Way disk, Milky Way halo, starburst galaxies, the circumgalactic medium and the intergalactic medium at low and high redshifts. We show that diffuse gas seen in such diverse environments can be simultaneously explained by a simple model of radiatively cooling gas. We show that most of such absorption line systems are consistent with being collisionally ionized, and estimate the maximum likelihood temperature of the gas in each observation. This model satisfactorily explains why O VI is regularly observed around star-forming low- z L* galaxies, and why N V is rarely seen around the same galaxies. We predict that the typical O VI column densities seen around these galaxies would be an order of magnitude higher than the associated N V column densities. We further present some consequences of this model in quantifying the dynamics of the cooling gas around galaxies and predict the shock velocities associated with such flows. Useful formulae for both observers and simulators are presented.

Subject headings: galaxies: evolution: general—galaxies: high-redshift—intergalactic medium—ISM: jets and outflows—quasars: absorption lines

1. INTRODUCTION

Quasar absorption line studies around galaxies, groups, clusters and of the intergalactic medium (IGM) are one of the most versatile techniques to detect gas which is otherwise too diffuse to be seen in emission. Observations of highly ionized diffuse gas (e.g. O VI, C IV, Ne VIII) in absorption have dramatically changed the way we look at a galaxy. Our current picture of galaxy evolution consists of a galaxy sitting at the center of a dark matter halo and a diffuse and large reservoir of cool and warm gas that envelopes the galaxy. These halos of diffuse gas, aptly named the circumgalactic medium (CGM) harbor large reservoir of gas that drive galaxy evolution (Tumlinson et al. 2011; Tripp et al. 2011; Bordoloi et al. 2014b; Peebles et al. 2014; Zhu & Ménard 2013a).

Recent progress of large scale galaxy surveys (York et al. 2000; Lilly et al. 2009), combined with the success of Ultraviolet spectroscopy with the Hubble Space Telescope (HST), have made it possible to systematically map the CGM and to correlate its properties with the host galaxy properties and the large-scale environment (Tumlinson et al. 2013; Stocke et al. 2013; Bordoloi et al. 2011; Chen et al. 2010; Prochaska et al. 2011; Zhu & Ménard 2013b; Werk et al. 2013; Stocke et al. 2014; Bordoloi et al. 2014a,b; Zhu et al. 2014; Borthakur et al. 2015). Tumlinson et al. (2011) showed that presence of diffuse O VI gas around a galaxy strongly depends on if the host galaxy is star-forming or not. There are also recent ob-

servations of O VI absorption detected in galaxy groups (Stocke et al. 2014; Johnson et al. 2015). These observations enable us to put lower limits on the CGM metal mass budgets by assuming a conservative maximum ionization fractions for the highly ionized species used in such calculations (Tumlinson et al. 2011; Bordoloi et al. 2014b). Knowing the true channel of ionization of such species would indeed reduce uncertainties in such metal mass estimates. It was found that the CGM of L* galaxies contain at least as much Oxygen as in their ISM Oxygen mass (Tumlinson et al. 2011). Similarly in the CGM of sub-L* galaxies, metal masses for Carbon in the CGM also likely exceed their ISM metal mass (Bordoloi et al. 2014b). Rare observations of diffuse Ne VIII gas around post-starburst galaxies suggest that “warm-hot” plasma might contain 10 to 150 times more mass than the cooler gas phases in post-starburst winds (Tripp et al. 2011).

Large absorption line surveys have utilized the Far Ultraviolet Spectroscopic Explorer (FUSE) telescope to study the hot diffuse “coronal” O VI gas present in the halo of the Milky Way (Sembach et al. 2003; Fox et al. 2006). They found that such diffuse “coronal” O VI is almost ubiquitously detected in the halo of the Milky Way. Fox et al. (2006) reported that 47 out of a total of 63 “highly ionized” absorbers are not associated with any 21 cm H I High Velocity Cloud emission in the halo of the Milky Way. They further report that 29 out of 38 O VI absorbers exhibit associated H I absorption seen in the Lyman series. Such observations have led many people to argue that the highly ionized gas may trace different phases of the diffuse halo gas, and ions such as O VI, Ne VIII, N V etc, might arise in collisionally-ionized gas (Fox et al. 2006; Lehner et al. 2011; Fox 2011). Wakker et al. (2012) compared the observations of highly ionized “coronal” gas such as O VI, Si IV, C IV to different

¹ MIT-Kavli Center for Astrophysics and Space Research, 77 Massachusetts Avenue, Cambridge, MA, 02139, USA; bordoloi@mit.edu

² Hubble Fellow

³ Department of Physics and Astronomy, John Hopkins University, 21218, Baltimore, MD

⁴ Space Telescope Science Institute, 3700 San Martin Drive, 21218, Baltimore, MD

theoretical models. They compared the column density ratios of such species to different models including models where the gas is in collisional ionization equilibrium (Gnat & Sternberg 2007), model of thick disk supernovae (Shelton 1998), shock ionization model (Dopita & Sutherland 1996), model of turbulent mixing layers (Slavin et al. 1993), models of static non-equilibrium ionization radiative cooling (Edgar & Chevalier 1986), conductive interface model (Borkowski et al. 1990), model of radiative cooling gas flow (Benjamin 1994) etc. Wakker et al. (2012) found that non-equilibrium ionization radiative cooling is important in producing such gas, but all the models fail to explain the full suite of observations. It is difficult to explain the ratio of N V to O VI column densities with a single density pure photoionization model (Werk et al. 2016 submitted).

Recent observations of circumgalactic and intergalactic O VI absorption at higher redshifts have made inferring the origin of such highly ionized absorption even more difficult. In CGM surveys such as COS-Halos (Tumlinson et al. 2013; Werk et al. 2013), it is seen that the warm O VI absorbers almost always have associated H I absorption. The kinematics of such H I gas suggest that they are typically cooler $< 10^5 K$ gas (Tumlinson et al. 2013). However, other observations have found that there are also rare examples where no H I gas is observed that is associated with the observed O VI absorption (Stocke et al. 2014). Further, increasing number of warm O VI absorbers with associated broad H I absorption is also being reported (Tripp et al. 2001; Savage et al. 2011). Savage et al. (2014) recently reported that 31% (14/45) of their sample of O VI absorbers lie in the temperature range of $5 < \log T < 6$.

In this work, we look at a simple model that can explain the available observations simultaneously and which can give insight into the origin of the gas around galaxies. Heckman et al. (2002) put forward a simple cooling flow model to explain the physical origin of such highly ionized diffuse absorbers. They argued that most of the observed O VI absorption-line systems could be explained as collisionally ionized gas radiatively cooling behind a shock or other type of radiatively-cooling flow. Our aim in this paper is to explore this cooling flow model further, and extend it to many other observations. This will help us to constrain the origin of these highly ionized absorption line systems.

This paper is organized as follows. In Section 2 we describe the observations that are used to compare with the cooling flow model. In Section 3 we describe the theory of cooling flow model for any radiatively cooling species. In section 4 we compare this model with observations. In Section 5 we describe the dynamics of the cooling gas, and finally in section 6 we summarize our findings.

2. THE OBSERVATIONS

In this section we list all the observations that have been compiled from literature to be used in this work. This compilation is not exhaustive and it is not meant to be a complete summary of all the observations to date. It is simply an extensive compilation of several works that represent observations covering a diverse range of environments: the disk of the Milky Way, the Milky Way halo, starburst galaxies, the low redshift IGM, the CGM around $z \approx 0.2$ L* galaxies, and the absorption lines de-

tected around $z \approx 2-3$ galaxies.

The primary measurements pertinent to our analysis are the column densities of various ionic species and their line widths (second moment of the line profiles). We use the Voigt profile column densities from literature and the fitted Doppler b (b_D) parameters, which is translated to line widths as $\Delta v = 3b_D/\sqrt{2}$. We consider data that have been published from the following works: the O VI data used for this work are collected from low and high redshift CGM studies of COS-Halos survey (Tumlinson et al. 2011), the KODIAQ survey (Lehner et al. 2014), observations of starburst galaxies Grimes et al. (2009), observations along the disk of the Milky Way (Bowen et al. 2008), and several IGM low and moderate redshift studies (Tripp et al. 2008; Meiring et al. 2013; Stocke et al. 2014; Savage et al. 2005; Burchett et al. 2015).

The Ne VIII doublet is harder to observe, as it has extremely blue rest frame wavelengths of 770.4 Å and 780.3 Å. There are only handful of detections of Ne VIII, primarily in high S/N HST/COS or FUSE spectra presented in several publications (Savage et al. 2005, 2011; Narayanan et al. 2009, 2011; Meiring et al. 2013; Hussain et al. 2015). We also include a new Ne VIII absorption detected towards QSO J1154+4635. This observation was done under HST PID (13852; PI Bordoloi). We detect O VI along with Ne VIII and H I along this sightline and the spectrum is shown as Figure A.1 in the Appendix. The measured O VI column density and Doppler line width for this absorber are $\log N_{OVI}/\text{cm}^{-2} = 14.71 \pm 0.03$, and $b_{OVI} = 99 \pm 11 \text{ km s}^{-1}$. The measured Ne VIII column density and Doppler line width for this absorber are $\log N_{NeVIII}/\text{cm}^{-2} = 14.65 \pm 0.08$, and $b_{NeVIII} = 187 \pm 39 \text{ km s}^{-1}$.

N V is not ubiquitously seen in the absorption line studies. We have compiled the handful of N V observations from COS-Halos (Werk et al. 2013), high redshift N V measurements associated with DLAs (Fox et al. 2009), low redshift IGM observations of (Savage et al. 2005; Burchett et al. 2015) and the Milky Way HVC observations of (Lehner et al. 2011).

Lastly, we present measurements of O VII absorption lines with high resolution *Chandra* and *XMM-Newton* spectra, that traces the warm and ionized gas of the Milky Way halo (Gupta et al. 2012). The O VII column densities were estimated using the curve of growth analysis. The low velocity resolution of the spectra made it impossible to directly measure the O VII line widths. Multiple absorption lines from the same ions were used to place limits on the column density and the Doppler b parameters of the O VII transitions (Gupta et al. 2012).

3. THEORY

In this section we briefly explain the cooling flow model for any radiatively cooling species that can be observed as an absorption line system. This theory is an update on the original work by (Heckman et al. 2002). Let us consider the situation in which gas cools radiatively from an initial temperature T and density n . The observed column density of any absorption line is given as

$$N = \int_{LOS} n dl \sim n L \quad (1)$$

Here the integration is performed over the path length (L) of the absorber. The total column density of a cooling gas is given by $N_{cool} = \dot{N}t_{cool}$, where t_{cool} is the cooling time and \dot{N} is the cooling rate per unit area. We can rewrite this expression as

$$N_{cool} = n t_{cool} v_{cool}, \quad (2)$$

where $v_{cool} = L_{cool}/t_{cool} = \dot{N}/n$. This characteristic cooling velocity v_{cool} might have different physical interpretations in different contexts. For example, if the gas is radiatively cooling behind a shock, the cooling velocity is the post-shock flow velocity in the region where that species exists. This is related to the cooling length $l_{cool} \sim v_{cool}t_{cool}$. If the gas is collapsing in a cooling instability, the characteristic size of the cooling region is $l_{cool} \sim c_s t_{cool}$. Here c_s is the isothermal sound speed ($\sqrt{P/\rho}$). In this case, the cooling velocity would be the sound speed. Generally in case of radiative cooling of gas at temperature T and metallicity Z ,

$$t_{cool} = \frac{3\kappa T}{n\Lambda(T, Z)}. \quad (3)$$

Using Equation 2, Equation 3 can be rewritten as

$$N_{cool} = \frac{3\kappa T}{\Lambda(T, Z)} v_{cool}. \quad (4)$$

This expression shows that N_{cool} is independent of density for radiative cooling. Moreover, at coronal temperatures radiative cooling is dominated by resonance lines due to metals. Thus, $N_{cool} \propto \Lambda^{-1} \propto Z^{-1}$. We now move on and write down the expression for the cooling flow column density for any arbitrary radiatively cooling metal X . Taking the ionic fraction of X at temperature T as $f_X(T)$ we get,

$$N_X = \frac{3\kappa T}{\Lambda(T_X, Z)} v_{cool} \left(\frac{X}{H} \right)_{\odot} Z f_X. \quad (5)$$

We know that $(\frac{X}{H}) \propto Z$, but also from the cooling function computed by Oppenheimer & Schaye (2013), we see that $\Lambda \propto Z$ for $Z > 0.1Z_{\odot}$. Hence for $Z > 0.1Z_{\odot}$, N_X is independent of metallicity. Throughout this work, we use the collisional ionization equilibrium (CIE) cooling function computed by Oppenheimer & Schaye (2013). Using 5 we can estimate the typical column density for O VI gas at a temperature ($T \approx 10^{5.5}$ K) where the ionic fraction of O VI is maximum ($f_{OVI} = 0.22$). This yields $N_{OVI} = 3.16 \times 10^{14} \text{ cm}^{-2}$ for $v_{cool} = 100 \text{ km s}^{-1}$.

Figure 1 shows the cooling flow column densities for various ionization states of Oxygen (blue squares), Neon (teal diamonds), Magnesium (red circles), Nitrogen (cyan crosses), Carbon (green diamonds) and Silicon (open diamonds), respectively. These column densities are computed at the temperature at which the ionic species has the maximum fractional abundance assuming collisional ionization equilibrium. The cooling velocity v_{cool} is assumed to be the isothermal speed of sound (C_s) for each species at that temperature. This figure presents the typical cooling column densities for each species at its peak fractional abundance temperature. This plot illustrates

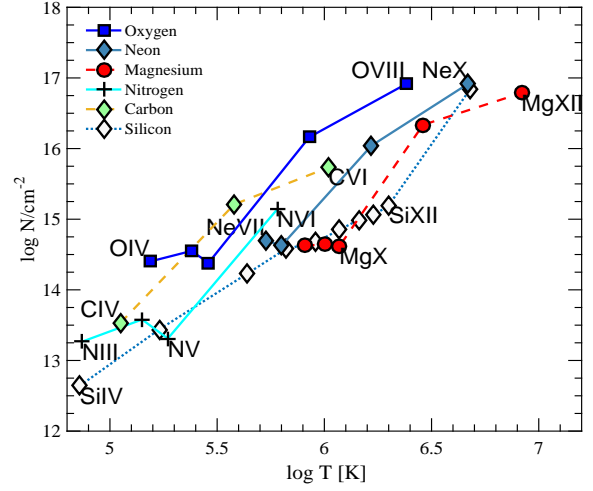


FIG. 1.— Model predictions for cooling flow column densities for several ions of abundant elements plotted at the temperature where each ion has its maximum fractional abundance assuming CIE. The model column densities are computed at the isothermal sound speed at that temperature.

how different species would have different column densities if they were produced by a gas flow that is radiatively cooling from $T \approx 10^7 \text{ K}$ at a velocity of $v_{cool} = C_s$ (i.e. Mach Number, $\mathcal{M}=1$). In such a cooling flow, the column density for O VI, Ne VIII and N V are $\log N_{OVI} = 14.4$, $\log N_{NeVIII} = 14.6$ and $\log N_{NV} = 13.3$, respectively. It is interesting to note that the column density predicted for N V is an order of magnitude smaller than that for O VI and Ne VIII.

Equation 5 shows that the cooling flow column density depends on the cooling temperature and the cooling velocity of that species. Hence we can represent equation 5 as a 2D surface, in temperature and velocity space. Figure 2 shows the cooling flow model predictions for four abundant species O VI, Ne VIII, Mg X and N V, respectively. We see that at a fixed temperature (assuming no thermal motion), the cooling column density and cooling velocities have almost a linear relationship. But at a fixed velocity, the cooling column density essentially depends on the fractional abundance of that species at CIE. At a given cooling velocity, the maximum cooling flow column density would always be observed at a temperature at which the fractional abundance of that species is maximum.

4. COMPARISON WITH DATA

In this section we study how the predictions of the cooling flow model column densities as given in equation 5, compare with real data. In order to compare the cooling flow model predictions with actual observations, we need to relate the observed line profile widths (Δv) to the cooling flow velocities. If there is no flow, the absorption lines would have a width purely due to thermal broadening given by $v_{th} = (2kT/m)^{1/2} \text{ km s}^{-1}$. However for radiatively cooling gas, the observed line width is due to a combination of pure thermal broadening as well as broadening due to cooling flow. We can write down Δv as a combination of cooling flow velocity, and thermal broadening.

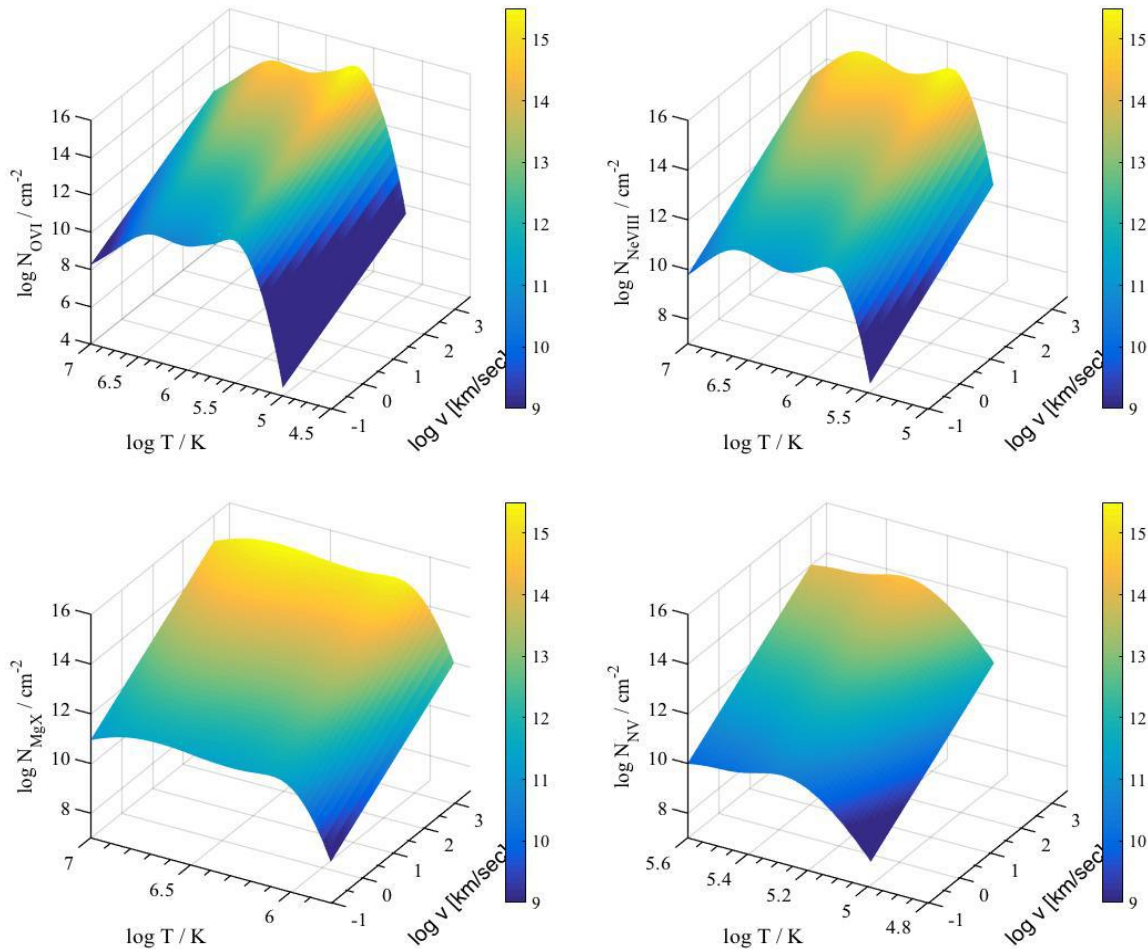


FIG. 2.— Cooling model prediction surfaces for O VI (top left), Ne VIII (top right), Mg X (bottom left) and N V (bottom right) respectively. At a fixed temperature the cooling flow column densities increase linearly with line width. At a fixed velocity the cooling flow column densities vary as a function of the fractional ionic abundance of that species.

$$\Delta v^2 = v_{cool}^2 + v_{th}^2. \quad (6)$$

To compare with models, we identify Δv with a line width that contains 99.7% (3σ) of the total absorption for any absorption line profile from its Voigt profile fit. This is described in the Appendix B. For any line profile quantified with a Voigt profile, and having a Doppler parameter b_D , we compute $\Delta v = 3b_D/\sqrt{2}$.

One issue that arises is how to relate the observed line width to the actual flow velocity. Simply put, the observed line width represents the spread in the flow velocity across the region where the column density of the particular ion is significant (rather than the flow velocity itself). We address this issue in Appendix B where we show that in a radiative shock the ratio of the line width and flow velocity is given by $\Delta v/v \sim \Delta T/T$ (the ratio of the range in temperature to the mean temperature in the region where the ionic column density is significant). This implies $\Delta v/v$ is of-order unity, justifying the use of the line width as an estimate of the flow velocity.

Figure 3 shows the comparison of the cooling flow column density predictions with observations for O VI, Ne VIII, N V, and O VII respectively. Figure 3, top left panel shows the O VI column densities and absorption

line widths as filled points, color coded to reflect the different studies from which they are collected. To compare to the model, we need to assume a column-density-weighted mean temperature for the observed ion. We denote these by $\langle T \rangle$.

The black lines in the top panel show the predicted cooling flow column densities for O VI at $\log \langle T \rangle = 5.5$ (the temperature at which fractional abundance of O VI is maximum) without thermal broadening (solid line) and with thermal broadening (dashed line), respectively. The dotted black line shows the predicted O VI cooling flow column densities at $\log \langle T \rangle = 6$. The different O VI absorption line systems define a clear relationship that spans over two decades in column densities and over one decade in line width. For absorbers with $\Delta v \gtrsim 30 \text{ km s}^{-1}$, the column density increases linearly with line width, while at lower line widths the column densities fall off sharply. Different O VI systems preferentially occupy different part of the diagram. The O VI systems associated with down the-barrel observations of starburst galaxies (red diamonds; Grimes et al. 2009), tend to have highest column densities and line widths, whereas hotter O VI gas possibly associated with an intra-group medium (cyan circles; Stocke et al. 2014), have lower column densities and smaller line widths.

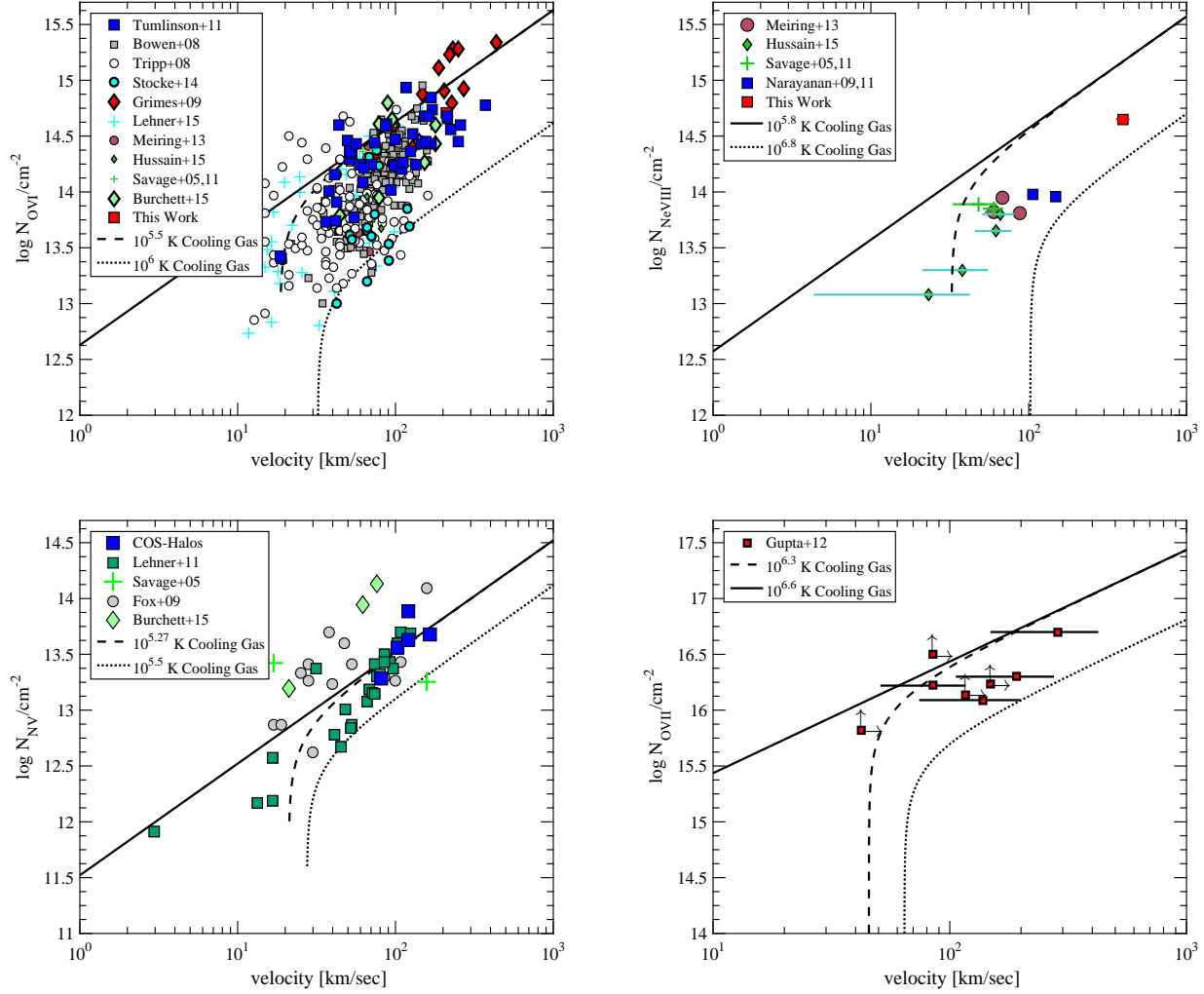


FIG. 3.— The distributions of observed O VI (top left panel), Ne VIII (top right panel), N V (bottom left panel), and O VII (bottom right panel) column densities vs line widths from literature. The black lines show the predicted cooling flow column densities at different temperatures, with (dashed and dotted lines) and without (solid lines) thermal broadening, respectively. The cooling flow models match the observations remarkably well for a range of observations.

Figure 3, top right (bottom left) panels show the same comparison for Ne VIII (N V). The black lines show the predicted cooling flow column densities for Ne VIII at $\log \langle T \rangle = 5.8$ and for N V at $\log \langle T \rangle = 5.27$ (temperatures at which their fractional abundances are maximum) without thermal broadening (solid lines) and with thermal broadening (dashed lines), respectively. The dotted black lines shows the predicted Ne VIII and N V cooling flow column densities at $\log \langle T \rangle = 6.8$ and $\log \langle T \rangle = 5.5$, respectively. Both Ne VIII and N V exhibit the correlation of increasing column density with increasing line width as seen for O VI gas.

It should be noted that for the COS-Halos survey, out of 26 detected O VI absorbers, only 3 lines of sight show associated N V absorption (Werk et al. 2013). This should not be taken as a sign that the CGM of star-forming L* galaxies have a sub-solar nitrogen/oxygen ratio. Our model predicts that the typical N V column densities should be an order of magnitude smaller than the O VI column densities at similar cooling velocities (see Figure 1). In the COS-Halos survey, the typical detection threshold is $\log N_{\text{X}} \gtrsim 13.5$. Hence most of the COS-Halos

N V systems that are associated with O VI absorption would reside below the detection threshold. All the COS-Halos N V detections are well explained by our model (Figure 3, bottom left panel). Moreover, higher signal to noise spectra from the Lechner et al. (2011) dataset show many more N V detections in the halo of the Milky Way. The high redshift N V systems detected by Fox et al. (2009) are associated with DLAs and broadly agree with our predictions, although a fraction of those N V absorbers lying above the solid black curve might be photoionized systems. However, most of the N V systems in Figure 3 are consistent with the predictions from a cooling flow model.

Finally, Figure 3, bottom right panel shows the O VII column density measurements (from X-ray spectroscopy), as a function of line widths. The arrows show the lower limits on column density and line width estimates and the range bars show the acceptable line widths from curve of growth analysis. The observations show very good agreement with the model, and most of the O VII absorbers lie in the linear regime of $N_{\text{OVII}}/\Delta v$ plot.

These models successfully reproduce the column den-

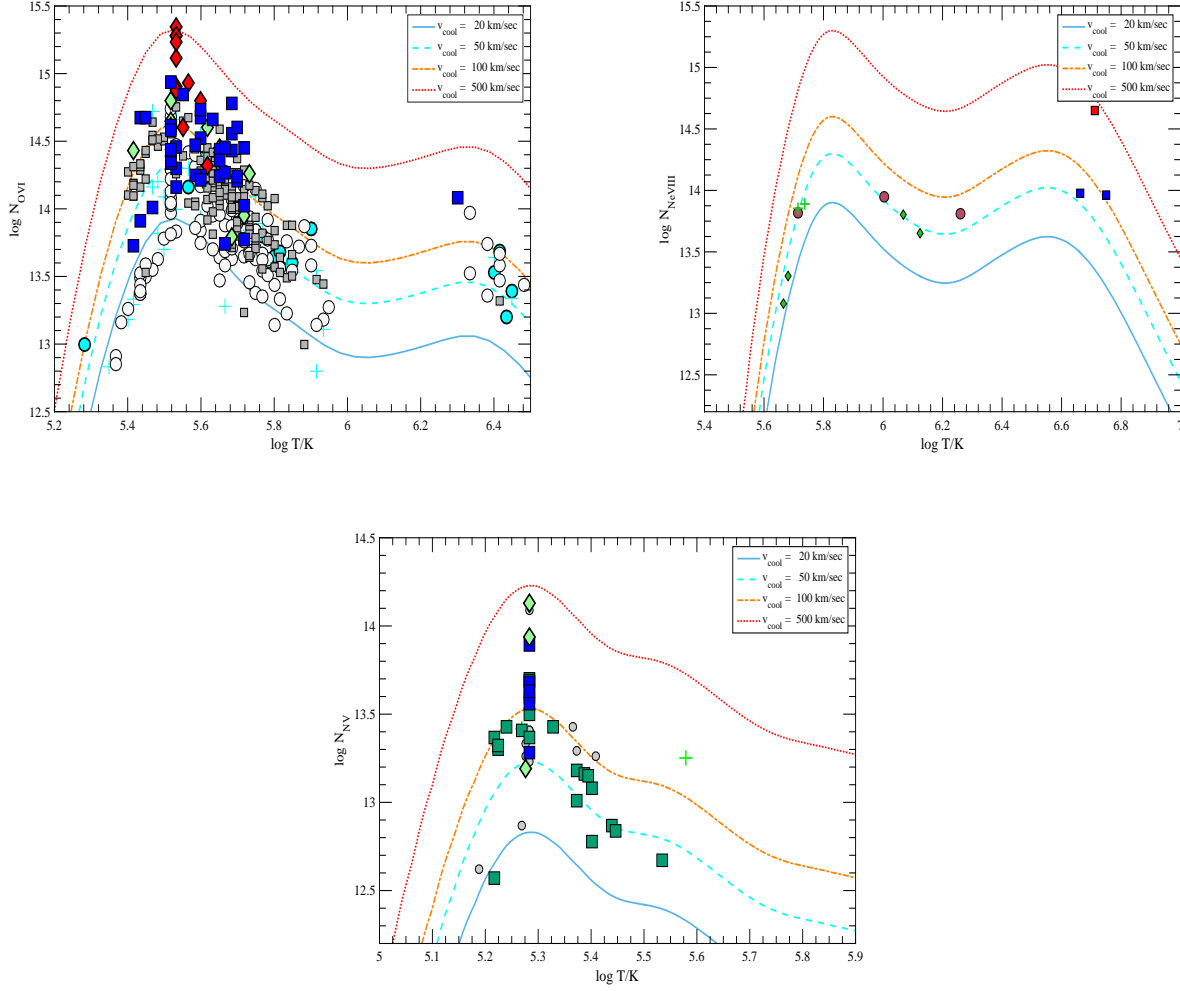


FIG. 4.— Maximum likelihood temperature estimates for O VI, Ne VIII and N V, measurements from observations. All literature observations with $\Delta v > 10 \text{ km s}^{-1}$ are included. The data points are color coded to reflect the different studies from which they are collected, as in Figure 3.

sity ranges where most of the observations lie for O VI, Ne VIII, N V, and O VII respectively. We should emphasize that the model has essentially no free parameters apart from $\langle T \rangle$ whose range of allowed values is set by simple physics. One more important feature of this model is that it naturally predicts the linear proportionality between the observed column density N_{obs} and Δv for all three species. When $\Delta v \gg v_{th}$, the values of $N_{obs}/\Delta v$ are in the linear regime, and when $\Delta v \gtrsim v_{th}$, there is a turn over in the ratio of $N_{obs}/\Delta v$. This can clearly be seen in Figure 3.

The loci of the model predictions as a function of $\langle T \rangle$ then encodes information about the values of the temperature $\langle T \rangle$, flow velocity, and column density of the absorbing gas for each absorbing system. However, we know that this is an idealized situation, where we are assuming that the cooling layers are moving with the same velocity and assume that there are no small scale motions inside the layers. In reality there might be turbulent mixing layers inside the cooling flows and there might be more than one layer of cooling flow along each line of sight. If these layers are physically close to each

other, they will never be seen at different velocities observationally. Moreover, as these observed column densities are not often saturated, these will be linearly added up and we will infer a wrong cooling velocity if we simply use their observed line broadening parameter as a proxy of v_{cool} .

We can model this effect as follows. Let us assume the simplest case where we have β plane parallel layers physically close to each other, all having the same cooling velocity v_{cool} . However, any observation will observe the linear sum of their individual column densities. Hence we can write down observed column density as

$$N_X = \sum_{i=1}^n N_{cool}^i, \quad (7)$$

$$N_X = \frac{3\kappa T}{\Lambda(T_X, Z)} \left(\frac{X}{H} \right)_{\odot} Z f_X \sum_{i=1}^n v_{cool}^i \quad (8)$$

Now Equation 6 can be rewritten as

$$\Delta v^2 = \beta^2 v_{cool}^2 + b_{th}^2. \quad (9)$$

This is the simplest case where v_{cool} is the same in all the layers, and β should increase with N_{OVI} . Ideally β should be integers, but any variation of β from integers simply means that there are higher order complexities which we are not accounting for here. We will not explicitly derive β . However, we can use this model to estimate the maximum likelihood temperature for each individual observations while treating β as a nuisance parameter. The probability of observing N_{obs} and Δv given the model can be written as

$$\mathcal{L} \equiv P(N_i, v_i | v, \beta, T) = \frac{1}{4\pi^2 \sigma_{N_i}^2 \sigma_{v_i}^2} \exp \left[\frac{-(N_{obs} - N_i)^2}{2\sigma_{N_i}^2} \right] \exp \left[\frac{-(\Delta v - v_i)^2}{2\sigma_{v_i}^2} \right] \quad (10)$$

We can marginalize over the multiplicity term β and Δv to compute the probability of any absorption system being at temperature T , given the observations as

$$P(T | N_i, v_i) = \int \mathcal{L} P(v, \beta, T) d\beta dv. \quad (11)$$

We assume a flat prior for cooling velocity, and the fractional distribution of the ion as a function of temperature as the prior on temperature. In a supersonic flow, the PDF of clouds are normally distributed (Wada & Norman 2007), hence we assume that the prior on β is a lognormal distribution centered on unity.

Figure 4 shows the maximum likelihood temperature estimates for O VI, Ne VIII, and N V measurements from the literature. The data points show the maximum likelihood measurements for each individual observation, and the colored lines show the predicted cooling flow model column densities at that given temperature for a fixed cooling velocity. The data points are color coded to reflect the different observations from which they are obtained, as in Figure 3. For O VI most of the measurements cluster around $\log \langle T \rangle \approx 5.5$, which is also the temperature at which the O VI fractional abundance is maximum. We also predict a small subsample of O VI absorbers to be at $\log \langle T \rangle \approx 6.4$, which are primarily lower column density and high Δv absorbers. For the handful of Ne VIII observations, we find a more scattered maximum likelihood temperature estimates, with most of the absorption lines being consistent with having $\log \langle T \rangle > 6$. For N V typical maximum likelihood temperatures are measured to be between $\log \langle T \rangle \approx 5.1$ to 5.6.

We conclude that this method allows us to estimate the temperature of the absorbing gas in an independent manner. It can also be applied to many other species and we can predict the typical cooling flow column densities that could be observed as a function of the temperature of the cooling gas. In Figure A.2 (Appendix C) we summarize our predictions for O IV, V, VII, C V, Ne V, VI, Mg X, and Si XII, respectively. Different lines in each panel represent the predicted column densities for different cooling velocities. The different velocity curves are assuming no thermal motion for this gas. All species

show a maximum cooling flow column density at a temperature where it has maximum fractional abundance. Some of the species can be observed with HST/COS UV spectroscopy, whereas some others can be accessed by X-Ray observations. Particularly for species like Mg X and O IV, we would be able to start comparing these model predictions with observations in the coming years, when new UV absorption line measurements will be published.

5. THE DYNAMICS OF THE COOLING GAS

One application of this cooling flow model is that it allows us to independently constrain the dynamics of the cooling gas. For a mass conserving cooling flow, we can write down the conservation equations as

$$\dot{M} = \rho v; \quad (12)$$

$$P + \dot{M}v = \Pi; \quad (13)$$

$$P = \rho \mathcal{R}T. \quad (14)$$

Here mass flux (\dot{M}) and momentum flux (Π) are conserved, and $\mathcal{R} = (k_B / \mu m_H)$. T is the temperature of the cooling gas, P is the pressure, ρ is the density and v is the velocity of the cooling flow at temperature T .

For a shock we also have

$$\Pi = \dot{M}v_{shock}. \quad (15)$$

These equations then yield

$$\frac{\Pi}{\dot{M}} = \frac{\mathcal{R}T}{v} + v = v_{shock}. \quad (16)$$

Thus, for any species, knowing the temperature and the cooling velocity, we can estimate the shock velocity associated with that cooling flow. Figure 5 shows the predicted shock velocities for cooling O VI gas at $\log \langle T \rangle = 5.3$ (solid blue curve), 5.5 (dashed cyan curve) and 6 (solid red curve), respectively. To compare with data, we are showing Δv along the x-axis, as defined by equation 6 (and see Appendix B). The estimated shock velocities from the O VI absorption line observations are shown as colored symbols. We can estimate the shock velocities as we have computed the maximum likelihood temperatures for these species as given in equation 11. The data points are color coded as in Figure 3 to identify the source of these measurements. The underlying contours show the distribution of the O VI velocities as compared to the model predictions. The bulk of the O VI measurements are found to have shock velocities at roughly $1.5C_s$ at $\log T \sim 5.5$. Therefore, bulk of the O VI gas is cooling behind supersonic shocks. The CGM O VI absorbers from COS-Halos (dark blue squares) and starburst galaxies (red diamonds), are in the winds cooling part of the diagram and they follow a linear relation with v_{shock} . The observations show very good agreement with model predictions (see underlying contours), as bulk of the O VI absorbers lie within the shock velocities predicted by typical O VI CIE temperatures.

To gain more insight, for an isothermal shock, equation 16 can be rewritten as

$$v_{shock} = v[1/(\mathcal{M}^2) + 1] \quad (17)$$

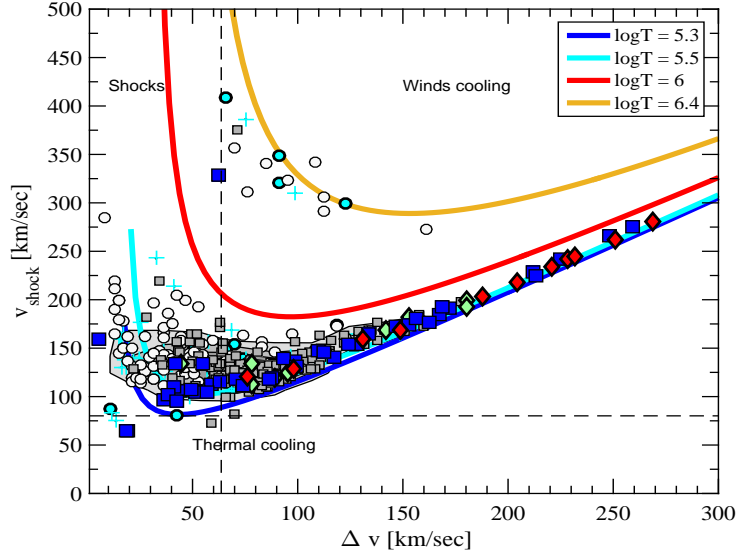


FIG. 5.— Estimated shock velocities for O VI measurements. The measurements are color coded as in Figure 3. The four solid lines show the estimated shock velocities at three different cooling temperatures. The underlying contours show the distribution of shock velocities for the O VI measurements.

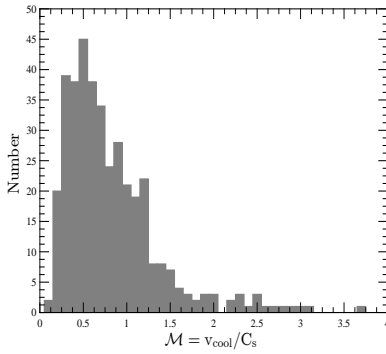


FIG. 6.— Histogram showing the Mach numbers (v/c_s) of the flow associated with each O VI observations with a temperature T . The bulk of the O VI absorbers are associated with a subsonic flow with a median Mach number of 0.7. The small fraction of O VI absorbers associated with supersonic flows are mostly arising in starburst winds seen down-the-barrel.

Here \mathcal{M} is the Mach number (v/c_s) of the flow at the location with temperature T . The curves in Figure 5 then represent loci along which the Mach number increases from the subsonic (upper left) to trans-sonic (near the curves minima) to supersonic (far right) regimes. We show this more explicitly in Figure 6. We see that the vast majority of cases are sub-sonic or trans-sonic. These would correspond to gas cooling through the O VI regime behind a shock. The typical shock velocities in these systems imply post-shock temperatures of $T_{shock} \sim 10^{5.2-5.8}$ K, high enough to produce O VI. The O VI absorbers associated with supersonic flows along the upper right branch are mostly arising in starburst winds. They are also associated with similar post shock temperatures as the subsonic cases.

A remarkable feature of Figure 5 are the minority of systems on the hot branch at $\log T = 6.4$. These are the higher temperature lines found in Lithium-like systems due to the O VI populated from higher ion states of O VII. Generally these are from hotter and therefore more mas-

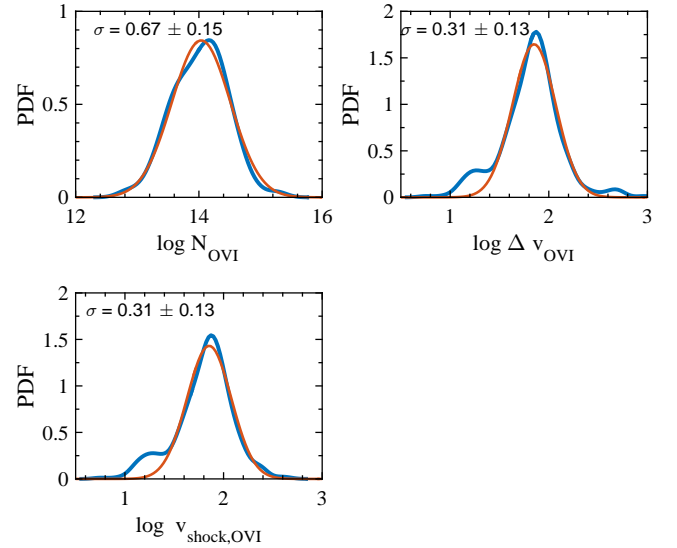


FIG. 7.— PDFs showing the distribution of all O VI measurements (blue curves). The O VI column density, velocities and derived shock velocities exhibit lognormal distributions. The fitted lognormal profiles are plotted as the thin brown lines.

sive systems. The total mass inferred from the hotter O VI systems would be much larger since the fraction of oxygen in this state is low relative to the cooler O VI lines. The open and cyan circles that constitute these hotter systems are found to be associated with the IGM and groups rather than with the general CGM. This then is a consistent physical picture.

As discussed in E we can derive species mass flow rates relative to the halo mass quite simply, and these are useful for cosmological simulations of galaxy formation since they can be compared with the accretion rates into halos now usually given relative to the halo mass (e.g. Behroozi & Silk 2015).

Figure 7, shows the kernel density estimated probability distribution functions (PDFs) for O VI observations. The distribution of the observed log column densities (top left panel), log of line widths (top right panel), and log of derived shock velocities (bottom left panel) and shown as blue curves. The PDFs can be well represented with lognormal distribution profiles (brown curves). The standard deviation of the distributions are listed on the top left corner of each plot. This classic PDF form occurs in both subsonic and also supersonic turbulence, and also in coagulation and condensation physics. Interacting cooler structures formed and given structure by many multiplicative processes such as we expect here naturally give such PDFs.

6. CONCLUSIONS AND DISCUSSIONS

Diffuse gas residing at warm ($T \sim 10^{5-6}$ K) temperature phase is important in many astrophysical contexts, but until recently it has been extremely difficult to observe. With the introduction of the HST/COS ultraviolet spectrograph, we have now a sizable sample of such warm absorbers to attempt a unified analysis of all such observations. In this paper, we show that O VI, Ne VIII, N V and, O VII absorption line systems, observed at diverse environments such as the Disk of the Milky Way, Milky Way halo, starburst galaxies, the circumgalactic medium and the intragroup medium at low and high redshifts, can be explained by a simple model where gas is in a radiatively cooling flow, such as behind a shock.

We collect a representative sample of O VI, Ne VIII, N V, and O VII absorption line systems from the literature and show that such absorbers exhibit a correlation between the observed $\log N$ of a species and the log of the line width of the same species. This relationship is linear for broad ($\Delta v \gtrsim 30 \text{ km s}^{-1}$) lines and turns over and steepens for narrower lines.

The model presented in this work can satisfactorily reproduce these observed column densities at their respective line widths. The column densities predicted by this model are independent of metallicity for any system that has $[\text{O}/\text{H}] > 0.1 [\text{O}/\text{H}]_{\odot}$. This model only depends on the characteristic speed of the cooling flow and can naturally explain both the shape and normalization of the observed column density and line widths for any highly ionized species. For any given highly ionized absorber at an observed column density and line width, we compute a maximum likelihood temperature associated with that absorber.

We are able to simultaneously explain absorption line systems observed in diverse environments and temperatures. This model naturally explains the ubiquitous presence of O VI around $z \sim 0.2$ star-forming L^* galaxies, and the surprisingly small strength of N V around the same set of galaxies in the COS-Halos survey. We predict that on average O VI should have an order of magnitude higher column density than N V. The detection threshold for the COS-Halos survey is such that most of the associated N V could not be detected due to lower S/N spectra. Along lines of sight with higher S/N spectra, probing the halo of the Milky Way, such N V systems are detected with higher frequency and are consistent with our model predictions.

We also present predictions for column densities that can be seen with other Li-like ions such as OIV, V, VII,

CV, NeV, VI, Mg X, and Mg XII. The small number of O VII observations are consistent with our model predictions. Future observations using HST/COS spectroscopy for the UV lines, or X-Ray absorption observations of the highly ionized hot gas will allow us to constrain this model further and test the origin of such absorption line systems.

This model allows us to independently constrain the dynamics of the cooling gas. In a mass conserving flow, at the maximum likelihood temperature of the O VI absorbers, we can compute the shock velocities associated with such flows. The absorption structures we observe associated with these shocks are likely two dimensional fractals that are sheet like. Observations show that the covering fraction of the O VI absorbers extends out to the virial radius of the halo (Johnson et al. 2015). The lower column density sheets we are observing with O VI may well be locked into the hot, X-ray emitting phase of the gas, if their Stokes numbers are low. In that case even gentle winds and feedback flows can keep these low column density structures aloft in the halo. As discussed more quantitatively in D, the Stokes number, St_i , of a species, X_i , is proportional to the ratio of the species column density, N_{X_i} , to the total halo column of (hot) gas. Low Stokes number allows the species, X_i , to be locked into the halo motions and to slow significantly any infall. This is why our highly ionized species are subsonic. Higher Stokes number will result in more rapid accretion. In general we expect the column densities of the CGM's cooler phase to decrease with increasing galactocentric radius.

The PDFs of the O VI absorption line structures as plotted in Figure 7 show a characteristic lognormal shape. This classic PDF form occurs in turbulence both subsonic and also supersonic and also in coagulation and condensation physics. Interacting cooler structures formed and given structure by many multiplicative processes such as we expect here naturally give such PDFs.

Our picture is that the CGM is a complex non-equilibrium system with a fractal like multiphase medium and with strong entropy flows due to heating, cooling and other feedback processes. The merit of the results given here is that we can now take out one uncertainty and robustly assume that in general O VI and similar ions are collisionally ionized. Our analysis also gives a transparent physical picture that modelers can incorporate and that observers can use in their analysis. The future challenge will be to undertake large surveys of higher ionization species such as Ne VIII, Mg X in absorption and deduce constraints on galaxy formation and CGM gas flows. Simultaneously, the next generation of integral field spectrographs such as MUSE and KCWI, will allow imaging of the gas structures we have inferred from the absorption line data. A clear next step is to incorporate all the known data systematically into our analysis and then design better cleaner diagnostic experiments.

7. ACKNOWLEDGMENT

Support for this work was provided by NASA through Hubble Fellowship grant #51354 awarded by the Space Telescope Science Institute, which is operated by the Association of Universities for Research in Astronomy, Inc., for NASA, under contract NAS 5-26555. This paper has greatly benefited from discussions with Guangtun

Ben Zhu, Claudia Scarlata, Andrew Fox. C.N. particularly acknowledges very many stimulating Galaxy Jour-

nal Club Friday lunchtime discussions with expert colleagues at STScI.

REFERENCES

- Behroozi, P. S. & Silk, J. 2015, *ApJ*, 799, 32
 Benjamin, R. A. 1994, PhD thesis, THE UNIVERSITY OF TEXAS AT AUSTIN.
 Bordoloi, R., Lilly, S. J., Kacprzak, G. G., & Churchill, C. W. 2014a, *ApJ*, 784, 108
 Bordoloi, R., et al. 2011, *ApJ*, 743, 10
 Bordoloi, R., et al. 2014b, *ApJ*, 796, 136
 Borkowski, K. J., Balbus, S. A., & Frstrom, C. C. 1990, *ApJ*, 355, 501
 Borthakur, S., et al. 2015, *ApJ*, 813, 46
 Bowen, D. V., et al. 2008, *ApJS*, 176, 59
 Burchett, J. N., Tripp, T. M., Prochaska, J. X., Werk, J. K., Tumlinson, J., O’Meara, J. M., Bordoloi, R., Katz, N., & Willmer, C. N. A. 2015, *ApJ*, 815, 91
 Chen, H., Helsby, J. E., Gauthier, J., Shectman, S. A., Thompson, I. B., & Tinker, J. L. 2010, *ApJ*, 714, 1521
 Correa, C. A., Wyithe, J. S. B., Schaye, J., & Duffy, A. R. 2015a, *MNRAS*, 450, 1514
 Correa, C. A., Wyithe, J. S. B., Schaye, J., & Duffy, A. R. 2015b, *MNRAS*, 450, 1521
 Correa, C. A., Wyithe, J. S. B., Schaye, J., & Duffy, A. R. 2015c, *MNRAS*, 452, 1217
 Dekel, A. & Krumholz, M. R. 2013, *MNRAS*, 432, 455
 Dopita, M. A. & Sutherland, R. S. 1996, *ApJS*, 102, 161
 Edgar, R. J. & Chevalier, R. A. 1986, *ApJL*, 310, L27
 Federrath, C. 2013, *MNRAS*, 436, 1245
 Federrath, C., Roman-Duval, J., Klessen, R. S., Schmidt, W., & Mac Low, M.-M. 2010, *A&A*, 512, A81
 Fox, A. J. 2011, *ApJ*, 730, 58
 Fox, A. J., Prochaska, J. X., Ledoux, C., Petitjean, P., Wolfe, A. M., & Srianand, R. 2009, *A&A*, 503, 731
 Fox, A. J., Savage, B. D., & Wakker, B. P. 2006, *ApJS*, 165, 229
 Gnat, O. & Sternberg, A. 2007, *ApJS*, 168, 213
 Grimes, J. P., Heckman, T., Aloisi, A., Calzetti, D., Leitherer, C., Martin, C. L., Meurer, G., Sembach, K., & Strickland, D. 2009, *ApJS*, 181, 272
 Gupta, A., Mathur, S., Krongold, Y., Nicastro, F., & Galeazzi, M. 2012, *ApJL*, 756, L8
 Heckman, T. M., Norman, C. A., Strickland, D. K., & Sembach, K. R. 2002, *ApJ*, 577, 691
 Hussain, T., Muzahid, S., Narayanan, A., Srianand, R., Wakker, B. P., Charlton, J. C., & Pathak, A. 2015, *MNRAS*, 446, 2444
 Johnson, S. D., Chen, H.-W., & Mulchaey, J. S. 2015, *MNRAS*, 449, 3263
 Lehner, N., O’Meara, J. M., Fox, A. J., Howk, J. C., Prochaska, J. X., Burns, V., & Armstrong, A. A. 2014, *ApJ*, 788, 119
 Lehner, N., Zech, W. F., Howk, J. C., & Savage, B. D. 2011, *ApJ*, 727, 46
 Lilly, S. J., et al. 2009, *ApJS*, 184, 218
 Meiring, J. D., Tripp, T. M., Werk, J. K., Howk, J. C., Jenkins, E. B., Prochaska, J. X., Lehner, N., & Sembach, K. R. 2013, *ApJ*, 767, 49
 Narayanan, A., Savage, B. D., Wakker, B. P., Danforth, C. W., Yao, Y., Keeney, B. A., Shull, J. M., Sembach, K. R., Froning, C. S., & Green, J. C. 2011, *ApJ*, 730, 15
 Narayanan, A., Wakker, B. P., & Savage, B. D. 2009, *ApJ*, 703, 74
 Oppenheimer, B. D. & Schaye, J. 2013, *MNRAS*, 434, 1043
 Peebles, M. S., Werk, J. K., Tumlinson, J., Oppenheimer, B. D., Prochaska, J. X., Katz, N., & Weinberg, D. H. 2014, *ApJ*, 786, 54
 Prochaska, J. X., Weiner, B., Chen, H.-W., Mulchaey, J., & Cooksey, K. 2011, *ApJ*, 740, 91
 Savage, B. D., Kim, T.-S., Wakker, B. P., Keeney, B., Shull, J. M., Stocke, J. T., & Green, J. C. 2014, *ApJS*, 212, 8
 Savage, B. D., Lehner, N., & Narayanan, A. 2011, *ApJ*, 743, 180
 Savage, B. D., Lehner, N., Wakker, B. P., Sembach, K. R., & Tripp, T. M. 2005, *ApJ*, 626, 776
 Sembach, K. R., Wakker, B. P., Savage, B. D., Richter, P., Meade, M., Shull, J. M., Jenkins, E. B., Sonneborn, G., & Moos, H. W. 2003, *ApJS*, 146, 165
 Shelton, R. L. 1998, *ApJ*, 504, 785
 Slavin, J. D., Shull, J. M., & Begelman, M. C. 1993, *ApJ*, 407, 83
 Stocke, J. T., Keeney, B. A., Danforth, C. W., Shull, J. M., Froning, C. S., Green, J. C., Penton, S. V., & Savage, B. D. 2013, *ApJ*, 763, 148
 Stocke, J. T., et al. 2014, *ArXiv e-prints*:1405.4307
 Tripp, T. M., Giroux, M. L., Stocke, J. T., Tumlinson, J., & Oegerle, W. R. 2001, *ApJ*, 563, 724
 Tripp, T. M., Sembach, K. R., Bowen, D. V., Savage, B. D., Jenkins, E. B., Lehner, N., & Richter, P. 2008, *ApJS*, 177, 39
 Tripp, T. M., et al. 2011, *Science*, 334, 952
 Tumlinson, J., et al. 2011, *Science*, 334, 948
 Tumlinson, J., et al. 2013, *ApJ*, 777, 59
 Wada, K. & Norman, C. A. 2007, *ApJ*, 660, 276
 Wakker, B. P., Savage, B. D., Fox, A. J., Benjamin, R. A., & Shapiro, P. R. 2012, *ApJ*, 749, 157
 Werk, J. K., Prochaska, J. X., Thom, C., Tumlinson, J., Tripp, T. M., O’Meara, J. M., & Peebles, M. S. 2013, *ApJS*, 204, 17
 York, D. G., et al. 2000, *AJ*, 120, 1579
 Zhu, G. & Ménard, B. 2013a, *ApJ*, 773, 16
 Zhu, G. & Ménard, B. 2013b, *ApJ*, 770, 130
 Zhu, G., et al. 2014, *MNRAS*, 439, 3139

APPENDIX

COS SPECTRUM

The HST-COS spectrum of a pair of new Ne VIII and O VI absorption lines and the associated Voigt profile fits are shown in Figure A.1. This was observed along QSO J1154+4635 under HST PID 13852 (PI: Bordoloi). The Voigt profile fitted column densities and line widths for O VI are $\log N_{\text{OVI}}/\text{cm}^{-2} = 14.71 \pm 0.03$, and $b_{\text{OVI}} = 99 \pm 11 \text{ km s}^{-1}$; for Ne VIII are $\log N_{\text{NeVIII}}/\text{cm}^{-2} = 14.65 \pm 0.08$, and $b_{\text{NeVIII}} = 187 \pm 39 \text{ km s}^{-1}$; and for H I are $\log N_{\text{HI}}/\text{cm}^{-2} = 16.73 \pm 0.02$, and $b_{\text{HI}} = 39 \pm 1 \text{ km s}^{-1}$, respectively.

RELATING OBSERVED LINE WIDTH TO COOLING VELOCITY

If we assume that a highly ionized species (e.g. O VI), is cooling behind a mass conserving shock wave; we can write down the following equations.

$$\dot{M} = \rho v; \quad (\text{B1})$$

$$P + \dot{M}v = \Pi; \quad (\text{B2})$$

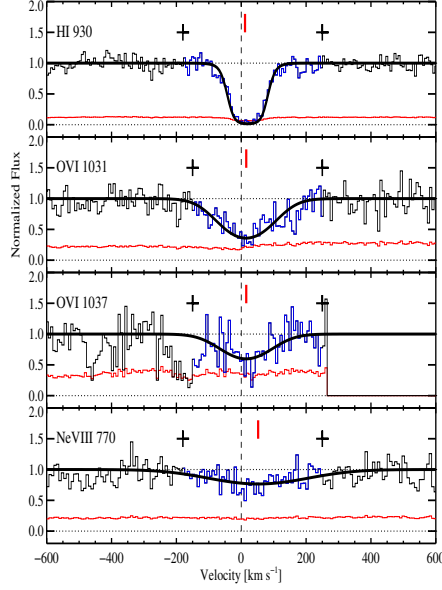


FIG. A.1.— An additional HST-COS quasar spectra of the H I, O VI and Ne VIII absorption lines with their corresponding Voigt profile fits (solid black line) are shown, which are included in this study. The vertical red ticks indicate the centroids of individual Voigt profile components and the black crosses show the velocity range over which the profile was integrated to compute their equivalent widths.

$$P = \rho \mathcal{R} T. \quad (\text{B3})$$

Here mass flux (\dot{M}) and momentum flux (Π) are conserved, and $\mathcal{R} = (k_B/\mu m_H)$. T is the temperature of the cooling gas, P is the pressure, ρ is the density and v is the velocity of the flow at temperature T . Combining these equations we can write

$$T = \frac{v[v_i - v]}{\mathcal{R}}; \quad (\text{B4})$$

where $v_i = \Pi/\dot{M}$. If the gas velocity in the post shock region is significantly slowed (i.e. if $v_i \gg v$), equation B4 becomes

$$T \sim \frac{v v_i}{\mathcal{R}}; \quad (\text{B5})$$

giving a linear relationship between T and v (lower T , lower v);

$$\frac{\Delta T}{T} \sim \frac{\Delta v}{v}. \quad (\text{B6})$$

This implies that the gas temperature behind the shock front would drop monotonically. Looking at the fractional ionization curve for O VI, we find that most of the O VI would exist in a temperature range of $\Delta T/T \sim \text{O}(1)$, and thus the width of the O VI line in velocity would be $\Delta v/v \sim \text{O}(1)$. In such a case the cooling velocity at temperature T is approximately the line width Δv as defined by equation 6. Thus we can understand that the cooling flow column density which involves multiplying by the cooling velocity can be accurately estimated by using the line width Δv as a proxy for the cooling velocity. A slightly more quantitative way to describe the relation between line width and flow velocity is to calculate, using the conservation laws, the relation between flow velocity, shock velocity and temperature obtaining for the logarithmic derivative, l , of flow velocity with respect to T :

$$l = \frac{\Delta \log v}{\Delta \log T} = \pm Y(1-Y)^{-1/2}(1 \pm (1-Y)^{1/2})^{-1} \quad (\text{B7})$$

with $Y = 4\mathcal{R}T/v_s^2$. As the shock varies between strong and weak the value of $|l|$ varies monotonically between $l = 3/2$ and $l = 1/2$. Thus the relation $\Delta v/v = l \Delta v/v$ helps justify the above assumption.

COOLING FLOW COLUMN DENSITY PREDICTIONS FOR SEVERAL SPECIES

In Figure A.2, we present the cooling flow model column density, temperature predictions for several species for which we do not compare the model to the data.

MASS ACCRETION RATE FROM CGM TO GALAXY

In general a turbulent supersonic (relative to the cool phase) multi-phase medium has a density PDF and column density PDF, $P(N)$ that is lognormal with a dispersion, $\sigma_i^2 = \log(1 + aM^2)$ where the parameter, a , is determined by

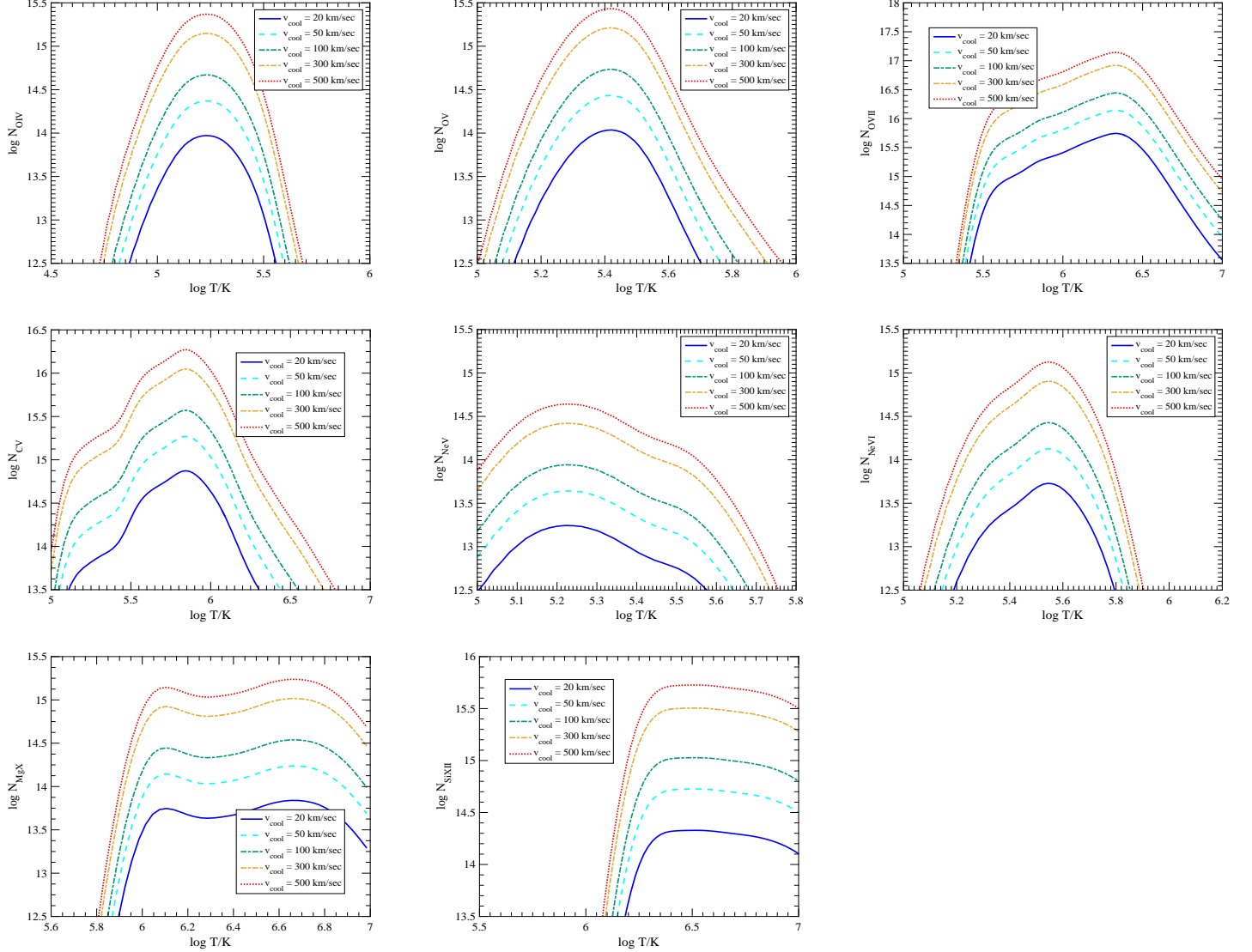


FIG. A.2.— Cooling flow column density estimates for various ionized species as a function of their corresponding cooling temperature. Different lines represent different cooling flow velocities.

solenoidal or compressible nature of the turbulence (Federrath et al. 2010; Federrath 2013). The Stokes number, St of a warm/cool-phase component e.g. O VI is given by $St = (\bar{\mu}_i N_{x_i} / N_{CGM})^{1/2}$ where $\bar{\mu}_i$ is the ratio of the molecular weights respectively and N_{CGM} is the total halo CGM halo column usually assumed to be mainly in hot gas. The cooling structures in the CGM are most likely fractal and more sheet like than spherical with dimension, d , somewhere around $d = 2.5$ as in diffusion limited accretion. The Low column density material stays in the upper halo but high column density clouds such as HVCs fall toward the galaxy at $St^{1/2} v_f$ where, v_f , is the free-fall velocity in the halo. A straightforward analysis give the effective accretion rate \dot{M}_{true} from halo to galaxy to be:

$$\dot{M}_{true} = \dot{M}_{cool} \frac{\sqrt{2}}{\pi} \int_{N_{crit}/\sqrt{2}\sigma_1}^{\infty} dx e^{-x^2} \quad (D1)$$

$$= \frac{1}{2} \dot{M}_{cool} k^{-1} K^{-3/2} \text{erf}[\log N_{crit}/\sqrt{2}\sigma_1] \quad (D2)$$

where N_{crit} corresponds to the Stokes number $St \sim 1$, \dot{M}_{cool} is the mass of the CGM gas and \dot{M}_{cool} is the CGM gas mass divided by its nominal cooling time, t_{cool} . The column densities are normalized to the median value as is usual with lognormal distributions. One way to physically analyze this is to assume that the unstable part of the cooling curve, $\Lambda(T)$ where O VI, N V, Ne VIII are present can be approximately fit by $\Lambda(T) = \Lambda_0 T^{-1/2}$. In the case the cooling time can be related to the entropy of the unstable cooling gas by $t_{cool} = kK^{3/2}$ where both Λ_0 , and k are known constants. The expression $\text{erf}(x)$ denotes the standard complementary error function with argument, x . The entropy, K , used

here is the standard astrophysical hot gas entropy $K = \kappa T / n^{2/3}$ for an ambient number density, n . There are then two ways to reduce the halo cooling time to a reasonable level consistent with the observations: (I) One can increase the entropy by feedback process due to star formation or AGN; (II) one can make the physically reasonable assumption that only Stokes numbers near $O(1)$ can accrete. Let us assume for example that $\log N_{crit} / \sqrt{2} \sigma_i = 2$ then the effective accretion rate is $\dot{M}_{true} \sim 1\% \dot{M}_{cool}$. Therefore we see that the feedback can operate via the turbulent energy input strongly influencing the multiphase CGM and slowing the infall by Stokes drag on the resulting cooling fractal-like “clouds” and “sheets”.

MASS FLOW RATES

From the gas cooling for species (i), we find the mass flow through the shock is given by:

$$\dot{M}_i = \Omega \pi R N_i (\mu_i m_h) x_i v \quad (E1)$$

where μ_i is the molecular weight of species, i . For the Lithium-like ions considered in this paper the covering factor is of order unity out to the virial radius and thus we take the value of the flow radius to be the virial radius i.e. $R = GM_{halo} / \sigma_{halo}^2$ where M_{halo} and σ_{halo} are the mass and velocity dispersion of the halo respectively. x_i is the correction factor for species i in its specific ionization state relative to the total abundance of i . A useful formula using 4 emerges using the analysis in the paper for the flow of species i (inflow or outflow):

$$\frac{\dot{M}_i}{M_{halo}} = G \Omega \pi (\mu_i m_h) x_i \frac{v^2}{\sigma_{halo}^2} \frac{\kappa T}{\Lambda(T)} \Big|_{T=T_i} \quad (E2)$$

Many papers relate the accretion onto the galaxy relative to the halo mass (Dekel & Krumholz 2013; Behroozi & Silk 2015; Correa et al. 2015a,b,c) and so this additional data point for the flow of the O VI and similar species is significant.